



Coexistence of interfacial stress and charge transfer in graphene oxide-based magnetic nanocomposites

Amodini Mishra¹, Vikash Kumar Singh², and Tanuja Mohanty^{1,*}

¹School of Physical Sciences, Jawaharlal Nehru University, New Delhi 110067, India

²Solid State Physics Laboratory, Timarpur, New Delhi 110054, India

Received: 3 January 2017

Accepted: 28 March 2017

Published online:

3 April 2017

© Springer Science+Business Media New York 2017

ABSTRACT

In this paper, the existence of both compressive stress and charge transfer process in hydrothermally synthesized cobalt ferrite–graphene oxide (CoFe₂O₄/GO) nanocomposites has been established. Transmission electron microscopy results reveal the decoration of CoFe₂O₄ nanoparticles on GO sheets. Magnetic response of nanocomposites was confirmed from superconducting quantum interference device magnetometer measurement. Optical properties of these nanocomposites were investigated by Raman spectroscopy. The interfacial compressive stress involved in this system has been evaluated from observed blue shift of characteristic G peak of graphene oxide. Increase in the full-width half-maximum value as well as upshift in D and G peaks is clear indications of involvement of charge transfer process between GO sheets and dispersed magnetic nanoparticles. The effect of charge transfer process is quantified in terms of shifting of Fermi energy level of these nanocomposites. This is evaluated from variation in contact surface potential difference using scanning Kelvin probe microscopy. XRD spectra of CoFe₂O₄/GO confirm the polycrystalline nature of CoFe₂O₄ nanoparticles. Lattice strain estimated from XRD peaks is correlated with the observed Raman shift.

Introduction

Graphene oxide (GO), a derivative of graphene, is an excellent two-dimensional (2D) flat sheet of hexagonally bonded *sp*² hybrid carbon atoms on which oxygen functional groups (such as hydroxyl, epoxide, carboxyl, carbonyl and hydroxyl groups) are covalently linked on their basal planes [1–6]. These functional groups attached to the negatively charged GO sheets can act as host for the positively charged ions

of nanoparticles (NPs) leading to the formation of nanocomposites. These nanocomposites exhibit unique properties as compared to individual components and therefore find a wide range of applications in surface-enhanced Raman scattering, sensors, catalysis and optoelectronic devices [7–10]. Nanocomposites synthesized by hydrothermal route are found to be in the form of dispersion of nucleated nanoparticles on GO sheets. It is a well known fact that magnetic nanoparticles (MNPs) have potential

Address correspondence to E-mail: tanujajnu@gmail.com; tmohanty@mail.jnu.ac.in

applications in the field of energy storage devices, MRI and magnetic field-driven drug delivery [11, 12]. Particularly, cobalt ferrite (CoFe_2O_4) NPs have found lots of applications in the field of catalysis and magnetism-based nanodevices due to their remarkable chemical and mechanical stability, magnetic behavior, low toxicity and biocompatibility in physiological environments [13–15]. However, pristine CoFe_2O_4 NPs suffers from irreversible aggregation and settling due to strong dipole–dipole interaction which can be overcome by employing viscoelastic carrier or surfactant. In this regard, two-dimensional (2D) planar structures like GO sheets are expected to solve this sedimentation problem by acting as a carrier which enhances the properties of CoFe_2O_4 NPs in nanocomposites form and expands its application possibilities with higher efficiencies in various fields like anode materials for Li-ion battery, electrochemical, photocatalysts, sensors, drug delivery, etc. [16–22].

In past few years, many groups have synthesized $\text{CoFe}_2\text{O}_4/\text{GO}$ nanocomposites and investigated their application possibilities in various fields [17–22]. However, studies on surface electronic, interfacial stress and charge transfer phenomenon of these materials are still unexplored. To the best of our knowledge, this is the first report which emphasizes on the existence of charge transfer as well as compressive stress in $\text{CoFe}_2\text{O}_4/\text{GO}$ magnetic nanocomposites which are confirmed from Raman spectroscopy, XRD and scanning Kelvin probe microscopy measurements. The surface electronic property, particularly shifting of Fermi surface, is monitored using scanning Kelvin probe microscopy, where it is measured in terms of variation in the contact surface potential difference (CPD). The morphology and structure of nanocomposites were examined using scanning electron microscopy and transmission electron microscopy. Their magnetic response was studied using superconducting quantum interference device (SQUID).

Experimental methods

Materials

Graphite flakes (99.8%, 325 mesh) were purchased from Alfa Aesar. Hydrazine hydrate (N_2H_4) and sulfuric acid (H_2SO_4 , 95%) were procured from

Sigma-Aldrich. Potassium permanganate (KMnO_4), sodium nitrate, (NaNO_3) hydrogen peroxide (H_2O_2), ethanol, hydrochloric acid (HCl), cobalt (II) nitrate hexahydrate [$\text{Co}(\text{NO}_3)_2 \cdot 6\text{H}_2\text{O}$], iron (III) nitrate nonahydrate [$\text{Fe}(\text{NO}_3)_3 \cdot 9\text{H}_2\text{O}$], ammonium hydroxide (NH_4OH) and double distilled water were purchased from Merck. All the chemicals have been used for experiment without further purification.

Synthesis of graphene oxide sheets

Graphene oxide (GO) was synthesized from graphite flakes using modified Hummers' method [23].

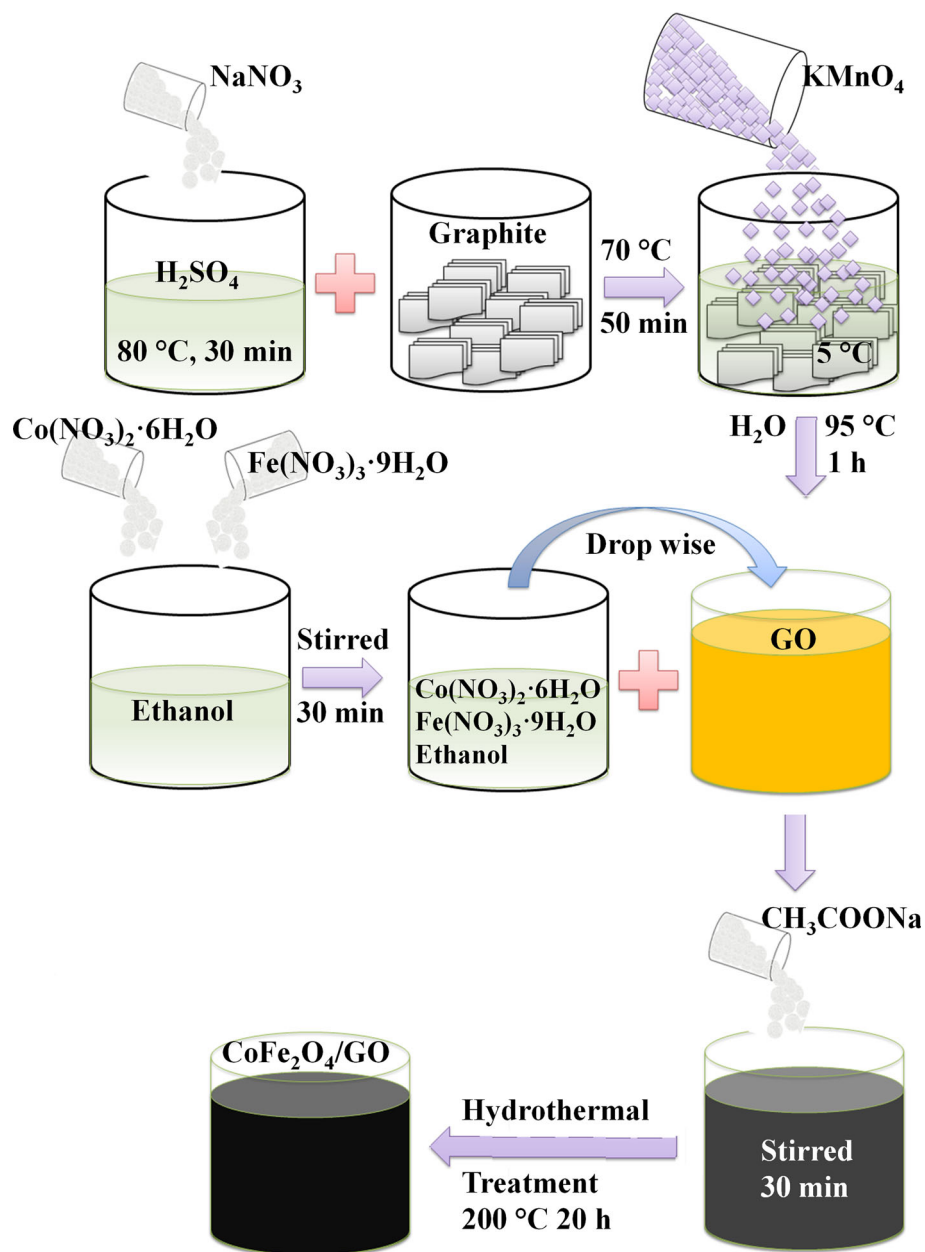
Synthesis of $\text{CoFe}_2\text{O}_4/\text{GO}$ nanocomposite

In the first step, graphene oxide (GO) was synthesized from graphite flakes using modified Hummers' method [23]. Graphene oxide-based cobalt ferrite nanocomposites ($\text{CoFe}_2\text{O}_4/\text{GO}$) were prepared by the hydrothermal method using cobalt (II) nitrate hexahydrate [$\text{Co}(\text{NO}_3)_2 \cdot 6\text{H}_2\text{O}$], iron(III) nitrate nonahydrate [$\text{Fe}(\text{NO}_3)_3 \cdot 9\text{H}_2\text{O}$] [16]. For this purpose, firstly 0.25 g of graphene oxide powder was added in 80 mL of ethanol and completely dispersed by ultrasonication for 60 min. In the second step, 0.3 g of $\text{Co}(\text{NO}_3)_2 \cdot 6\text{H}_2\text{O}$ and 0.9 g of $\text{Fe}(\text{NO}_3)_3 \cdot 9\text{H}_2\text{O}$ were dissolved in 50 mL of ethanol followed by stirring for 3 h. The solution was mixed dropwise into the GO suspension with continuous stirring for 5 h. After that, 4.3 g of sodium acetate (CH_3COONa) was added into the mixture under continuous stirring. After agitation for 8 h, the mixture solution was transferred to a Teflon-line autoclave. The autoclave was heated under oven at 200 °C for 24 h and then cooled down to room temperature. The solid product was separated by centrifugation and washed thoroughly with water and absolute ethanol to remove impurities. Finally, the product was dried in an oven at 50 °C for a 12 h. The final product was labeled as graphene oxide-based cobalt ferrite nanocomposites ($\text{CoFe}_2\text{O}_4/\text{GO}$). The steps involved during synthesis process of $\text{CoFe}_2\text{O}_4/\text{GO}$ nanocomposites are schematically illustrated in Fig. 1.

Characterization

The surface morphology of GO and $\text{CoFe}_2\text{O}_4/\text{GO}$ was investigated by scanning electron microscopy (SEM) (Zeiss EVO-40, working voltage 20 kV,

Figure 1 Schematic representation of steps involved in the synthesis of $\text{CoFe}_2\text{O}_4/\text{GO}$ nanocomposites.



Germany). The elemental identification of $\text{CoFe}_2\text{O}_4/\text{GO}$ nanocomposites was confirmed from energy-dispersive X-ray analysis (EDAX). EDAX measurement was carried out using a (Zeiss EVO ED15) microscope coupled with an (Oxford-X-MaxN) EDX detector. The magnetic properties of the nanocomposites were investigated at room temperature using a Quantum Design MPMS-7 SQUID magnetometer. From the magnetization versus applied field plot ($M-H$), the saturation magnetization (M_s), coercivity (H_c) and remanence magnetization (M_r) were determined. For structural analysis, transmission electron

microscopy study was carried out by 200 kV TEM (JEOL 2100F, Japan). X-ray diffraction (XRD) spectra of $\text{CoFe}_2\text{O}_4/\text{GO}$ nanocomposites samples were recorded using an X-ray diffractometer (PANalytical 2550-PC X-ray diffractometer). XRD data were collected using CuK_α ($\lambda = 0.154\text{ nm}$) radiation with 2θ ranging from 10° to 70° at scanning rate 3° min^{-1} . Optical properties of GO and $\text{CoFe}_2\text{O}_4/\text{GO}$ nanocomposites were investigated using Raman spectroscopy (HORIBA Xplora) having green laser ($\lambda = 514\text{ nm}$) excitation with a laser spot size $1\text{ }\mu\text{m}$. The effect of CoFe_2O_4 nanoparticles decoration on the

Fermi energy level of GO sheets was monitored by scanning Kelvin probe microscopy (SKPM, KP Technology, UK).

Results and discussion

SEM and EDAX studies

SEM image and EDAX spectra analysis of GO and $\text{CoFe}_2\text{O}_4/\text{GO}$ nanocomposites thin films were carried out for observation of the surface morphology and identification of the elements present in the GO and $\text{CoFe}_2\text{O}_4/\text{GO}$ nanocomposites as shown in Fig. 2. In the SEM image of GO, crumpled sheets like structures are observed which are common for graphene or graphene oxide when deposited on a substrate [24]. On the other hand, in the case of $\text{CoFe}_2\text{O}_4/\text{GO}$ nanocomposites, well-dispersed CoFe_2O_4 nanoparticles on GO sheet are found.

EDAX spectrum of GO sheets confirms the presence of C, O and Si elements, and that of $\text{CoFe}_2\text{O}_4/\text{GO}$ nanocomposites indicates the prominent presence of C, O, Co, Fe and Si elements. Additional Si peak arising in both the cases is from the silicon substrate. The peaks in the EDAX pattern were

assigned to the elements present in $\text{CoFe}_2\text{O}_4/\text{GO}$ composites EDAX spectra of GO and $\text{CoFe}_2\text{O}_4/\text{GO}$ nanocomposites clearly signify the high purity in chemical composition of $\text{CoFe}_2\text{O}_4/\text{GO}$ nanocomposites.

SQUID measurement

Magnetic properties of the nanocomposites were investigated using a SQUID. The $M-H$ loop for the $\text{CoFe}_2\text{O}_4/\text{GO}$ nanocomposites at 300 K (room temperature) is shown in Fig. 3a. At room temperature, the value of saturation magnetization ' M_s ' comes out to be 75.37 emu/g which is lower than that of corresponding pure bulk CoFe_2O_4 (94 emu/g). The remanence magnitude ' M_r ' extracted from the hysteresis loop at the intersections of the loop (shown in the inset of Fig. 3a) with the vertical magnetization axis is found to be 20.05 emu/g. The coercivity H_c obtained from hysteresis loop is 0.41 kOe for as-prepared $\text{CoFe}_2\text{O}_4/\text{GO}$ nanocomposites [25, 26] which is quite low, thus indicating its soft magnetic nature. The steep rise of $M-H$ loop indicates the superparamagnetic behavior of these $\text{CoFe}_2\text{O}_4/\text{GO}$ nanocomposites having small remnant magnetization and coercivity. Superparamagnetism behavior of these

Figure 2 SEM images of **a** GO, **b** $\text{CoFe}_2\text{O}_4/\text{GO}$ nanocomposites and EDAX spectrum of **c** GO and **d** $\text{CoFe}_2\text{O}_4/\text{GO}$ nanocomposites.

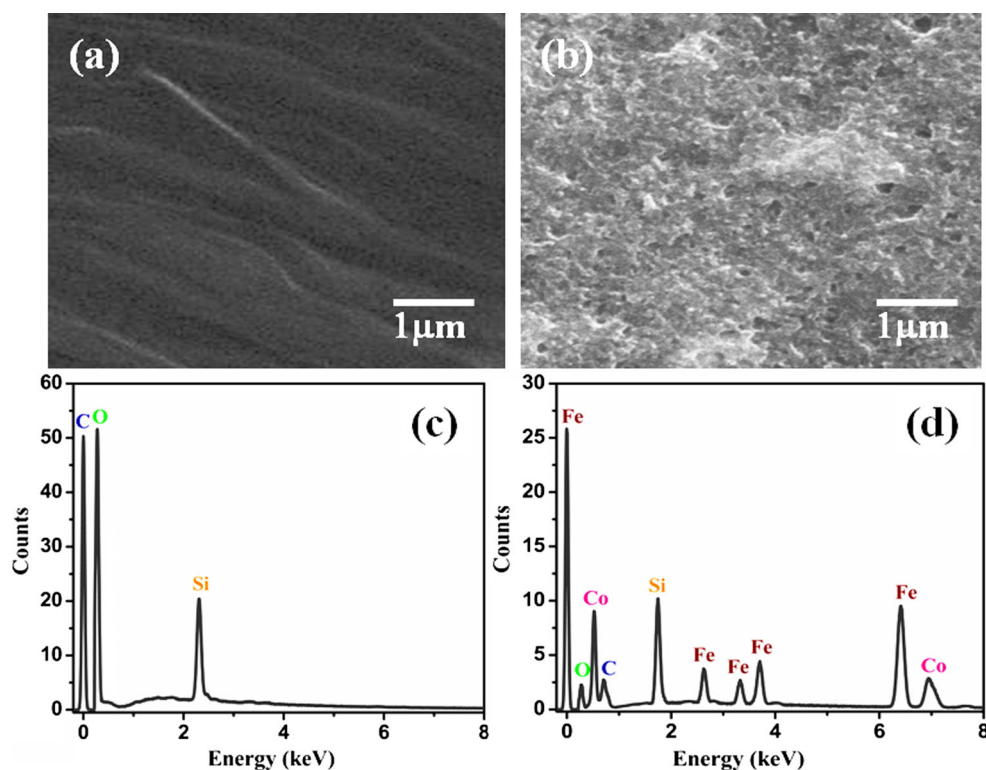
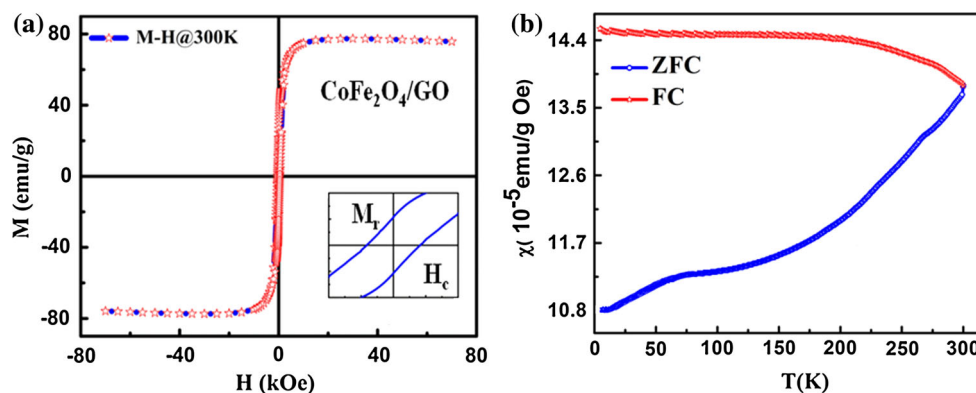


Figure 3 **a** Hysteresis loop (M – H) of $\text{CoFe}_2\text{O}_4/\text{GO}$ nanocomposites at room temperature 300 K (*inset* zoom M – H loop of $\text{CoFe}_2\text{O}_4/\text{GO}$ nanocomposites at 300 K). **b** The plot of χ versus T of zero-field cooling (ZFC) and field cooling (FC) for $\text{CoFe}_2\text{O}_4/\text{GO}$ nanocomposites.



nanocomposites eliminates the possibility of magnetic clustering with negligible magnetic interactions, thus opening up many possibilities of applications of these nanocomposites in the field of sensors, Li-ion battery, photocatalysts, etc.

Further, the presence of superparamagnetic particles was also examined using zero-field-cooling (ZFC) and field-cooling (FC) measurements with an applied magnetic field of 100 Oe. The magnetic susceptibility (χ) versus temperature plot for $\text{CoFe}_2\text{O}_4/\text{GO}$ nanocomposites is shown in Fig. 3b. For the zero-field-cooled (ZFC) case, the sample was cooled from 300 K to 2 K and then a magnetic field ($H = 100$ Oe) was turned on for magnetization (M) measurements with increasing temperature after ensuring stabilization at each temperature. Upon reaching 300 K, the data were similarly collected with decreasing temperature (FC mode) keeping the same applied field. It is clear that FC and ZFC curves show divergence at around 300 K which can be considered as the blocking temperature (T_b) above which it is superparamagnetic in nature [27, 28]. The magnetic moments follow the direction of the applied magnetic field resulting in low remanence and low coercivity which are the characteristic features of superparamagnetism.

TEM studies

Microstructure analysis of these composites was carried out using TEM for which in the first step, ethanol-based solutions of GO and $\text{CoFe}_2\text{O}_4/\text{GO}$ were placed on carbon-coated copper grids followed by drying at room temperature. TEM images of GO and $\text{CoFe}_2\text{O}_4/\text{GO}$ nanocomposites are shown in Fig. 4a, b, respectively. Figure 4a corresponds to the appearance of thin and wrinkled transparent GO

sheets. It is consistent with our observation from the SEM analysis confirming the layer morphology of graphene oxide. Figure 4b exhibits well dispersion of CoFe_2O_4 NPs on GO sheets. The sheet-like corrugated morphology of GO is also well preserved in $\text{CoFe}_2\text{O}_4/\text{GO}$ nanocomposites, and CoFe_2O_4 NPs are dispersed on GO sheet. This type of nucleation of magnetic nanoparticles on GO sheets is expected from hydrothermal synthesis. The nanoparticles are evenly distributed on the GO sheets without significant agglomeration. The average particles size of CoFe_2O_4 nanoparticles in $\text{CoFe}_2\text{O}_4/\text{GO}$ nanocomposites is about 18 ± 2 nm. The line spacing in crystalline (311) plane of CoFe_2O_4 is found to be 0.24 nm from high-resolution TEM (HRTEM) image (Fig. 4c) The selected area electron diffraction (SAED) pattern of $\text{CoFe}_2\text{O}_4/\text{GO}$ nanocomposites is shown in Fig. 4d, where the diffraction rings corresponding to the planes (111), (220) and (311) of CoFe_2O_4 as well as a diffraction pattern corresponding to hexagonally arranged carbon atoms in GO sheets are observed.

XRD measurement

$\text{CoFe}_2\text{O}_4/\text{GO}$ nanocomposites thin films were characterized by XRD (PANalytical 2550-PC X-ray diffractometer) setup using CuK_α radiation ($\lambda = 0.154$ nm). The data were collected between scattering angles (2θ) from 10° to 70° at scanning rate 3° min^{-1} . The crystalline nature of $\text{CoFe}_2\text{O}_4/\text{GO}$ nanocomposites was confirmed from its X-ray diffraction (XRD) spectra as shown in Fig. 5a.

The XRD spectrum of $\text{CoFe}_2\text{O}_4/\text{GO}$ nanocomposites exhibits polycrystalline nature of CoFe_2O_4 NPs having a characteristic peak at $2\theta = 35.6^\circ$ in addition to other peaks of CoFe_2O_4 appearing at $2\theta = 18.7^\circ$ (111), 30.1° (220), 35.6° (311), 43.2° (400), 54.1° (422), 57.3° (511) and

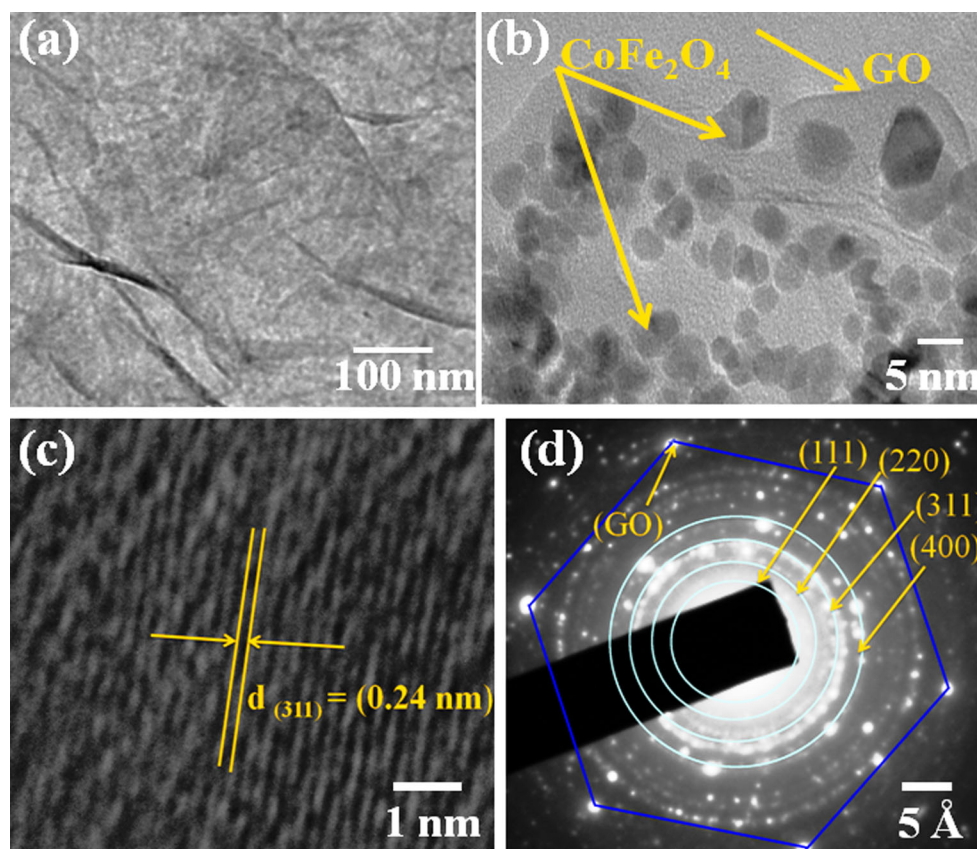


Figure 4 TEM images of **a** GO sheets, **b** CoFe₂O₄/GO nanocomposites, **c** HRTEM of CoFe₂O₄ nanoparticles lying on GO sheets and **d** selected area diffraction pattern of CoFe₂O₄/GO nanocomposites.

62.9° (440) (JCPDS no. 75-0033). Nucleation of CoFe₂O₄ nanoparticles is expected to induce strain in GO sheets. For calculation of the crystalline sizes and lattice strain in the nanocomposites, Williamson–Hall (W–H) peak-broadening analysis was used assuming peak widths as a function of 2θ .

The strain induced in powder due to crystal imperfection and distortion is calculated using the formula

$$\Delta\xi/\xi = \frac{\beta}{\tan\theta} \quad (1)$$

where β is full-width half-maximum (FWHM) of diffraction peak (in radian), θ is Bragg's diffraction angle (in degree), and $\Delta\xi/\xi$ is lattice strain. The crystallite size was calculated from the X-ray diffraction spectra using Scherrer's formula, where the crystallite size is inversely related to $\beta \cos\theta$. Consider the fact that particle size and strain are independent of each other having a Cauchy-like form, which in combination are related to FWHM by W–H equation as follows

$$\beta \cos\theta = \frac{K\lambda}{D} + \frac{\Delta\xi}{\xi} \sin\theta \quad (2)$$

where the term $K\lambda/D$ represents the Scherrer's particle size distribution [29, 30]. Figure 5b shows the W–H plot for CoFe₂O₄/GO nanocomposites. A linear least-square fitting (5% error) to $\beta \cos\theta$ versus $\sin\theta$ data plot yields the value of average crystallite size (D) and lattice strain ($\Delta\xi/\xi$) to be 17 nm and 0.003, respectively. The crystallite size is in good agreement with the observed size of crystallites from TEM measurement, and lattice strain is expected to be compressive type which will be discussed in forthcoming section.

Raman studies

In the present study, the Raman spectra of GO sheets and CoFe₂O₄/GO nanocomposites are recorded by using Raman spectrometer, and the spectra are shown in Fig. 6. The main features in the Raman spectra of graphene oxide sheets are D and G peaks located at 1345 and 1587 cm⁻¹, respectively. From

Figure 5 **a** XRD spectrum (inset showing XRD peak of GO) and **b** Williamson–Hall plot (linearly fitted $\beta \cos\theta$ versus $\sin\theta$ data) for $\text{CoFe}_2\text{O}_4/\text{GO}$ nanocomposites.

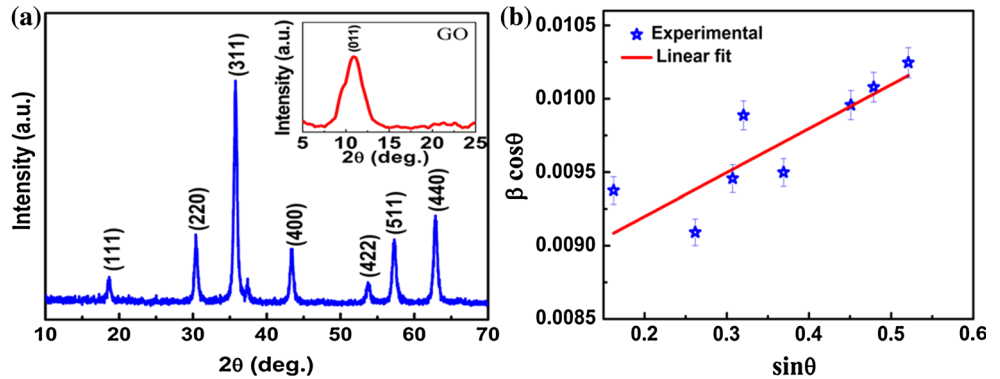


Fig. 6, it is observed that there is a decrease in the intensity of D and G peaks of GO after decoration of CoFe_2O_4 nanoparticles on GO. This is due to decrease in the exposure area of GO sheets in $\text{CoFe}_2\text{O}_4/\text{GO}$ nanocomposites to excitation light in Raman measurement. This was confirmed from SEM and TEM measurements. G band is attributed to the Brillouin zone-centered LO and $i\text{TO}$ phonon mode. D band is attributed to the double-resonance excitation of phonons close to the K point scattering due to defects on $i\text{TO}$ (E_{2g}) phonon in the Brillouin zone [28].

The Raman spectrum of $\text{CoFe}_2\text{O}_4/\text{GO}$ nanocomposites shows a distinct broadening of the D and G peaks of GO sheets from a full-width half-maximum (FWHM) of 122–165 and 69–77 cm^{-1} , respectively, which is due to lattice strain stemming from the interaction between GO sheets and CoFe_2O_4 magnetic nanoparticles [31, 32]. The Raman spectrum of $\text{CoFe}_2\text{O}_4/\text{GO}$ nanocomposites shows an upshift in Raman peaks position of D and G peaks as compared

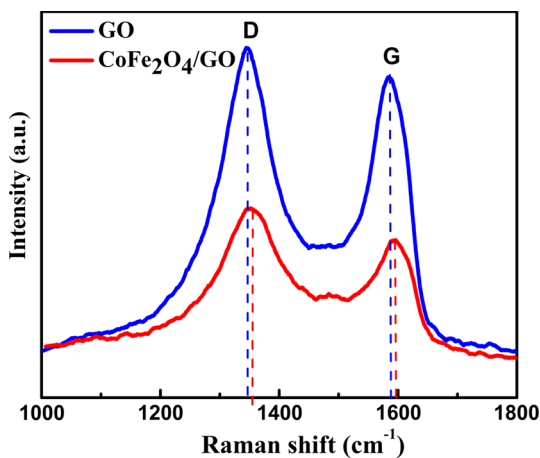


Figure 6 Raman spectra of GO sheets and $\text{CoFe}_2\text{O}_4/\text{GO}$ nanocomposites.

to GO sheets. The D peak is shifted from 1345 to 1354 cm^{-1} , while the G peak is shifted from 1587 to 1595 cm^{-1} (Fig. 6). This is unlike to the reported observation of red shift in case of graphene oxide-based polymer nanocomposites [33].

The observed shift in Raman spectrum of graphene oxide is similar to that found in graphene when subjected to lattice strain. Strain can be due to stretch in carbon–carbon bond or symmetry breaking or anisotropy in the lattice [34]. Also, residual stresses arising from differential contraction of the GO and magnetic material during drying period could have contributed to the blue shift in Raman peak [35]. The direction of shift in Raman G peak is dependent on the nature of strain. Blue shift in G peak can be assigned to interfacial compressive strain. The local strain can be explained in terms of a schematic/model to understand the observed blue shift of the Raman D and G peaks in $\text{CoFe}_2\text{O}_4/\text{GO}$ (Fig. 7). The schematic shown in Fig. 7 is a depiction of TEM images where nanocomposites of $\text{CoFe}_2\text{O}_4/\text{GO}$ are in the form of decoration of CoFe_2O_4 nanoparticles on GO sheets. Lattice mismatch and disorder are expected to produce compressive stress on few layers of graphene oxide resulting in close packing of surface atoms which could have led to the scattering at higher vibrational wavenumber.

In Raman spectra, significant blue shift observed in D and G peaks may be attributed to simultaneous contribution from interfacial stress as well as from charge transfer process. Compressive strain involved in these van der Waal systems could have arisen from lattice mismatch between CoFe_2O_4 nanocrystallites and GO flakes resulting in upshift in G peak. The role of defects introduced during synthesis of $\text{CoFe}_2\text{O}_4/\text{GO}$ nanocomposites also cannot be ruled out. The existence of strain is also confirmed by XRD studies

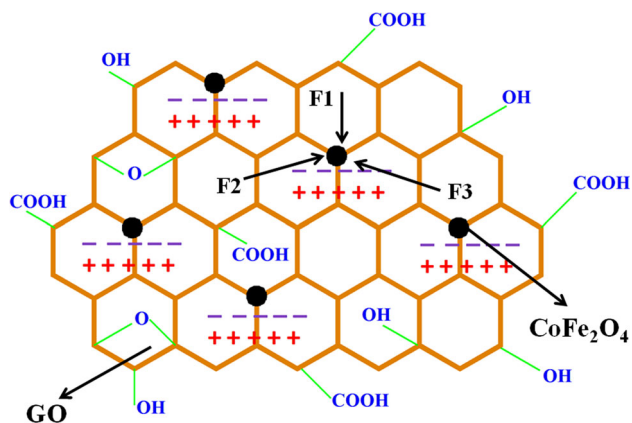


Figure 7 Schematic illustration of interfacial compressive stress involved in $\text{CoFe}_2\text{O}_4/\text{GO}$ nanocomposites.

as shown in Fig. 5b. In our previous studies, similar type of blue shift in Raman E_{2g} phonon is observed in the case of $\text{Fe}_3\text{O}_4/\text{GO}$ nanocomposites. [36]

For a hexagonal system like graphene oxide, the strain can be expressed in terms of interfacial stress (σ) as

$$\omega_\sigma - \omega_0 = \alpha\sigma \quad (3)$$

where $\alpha = A (S_{11} + S_{12})/\omega_0$ is the stress coefficient for Raman shift and σ is the compressive stress. A is a constant, and S_{11} and S_{12} are graphite elastic constants having values as $A = -1.44 \times 10^{-7} \text{ cm}^{-2}$, $S_{11} = 0.98 \times 10^{-12} \text{ Pa}^{-1}$, $S_{12} = -0.16 \times 10^{-12} \text{ Pa}^{-1}$, respectively [37]. ω_σ and ω_0 are frequencies of Raman E_{2g} phonon under stressed and unstressed conditions, respectively. Using these constants, in Eq. (3), Raman shift of 8 cm^{-1} in G peak of $\text{CoFe}_2\text{O}_4/\text{GO}$ corresponds to the stress coefficient (α) and compressive stress (σ) to be 7.46 cm^{-1} and 1.07 GPa , respectively. We suggest that this stress might have arisen due to lattice mismatch as well as increase in defect concentration. The amount of defects present in the sample can be quantified by measuring the ratio (I_D/I_G) of the D and G bands. The value of I_D/I_G for GO sheets and $\text{CoFe}_2\text{O}_4/\text{GO}$ nanocomposites is found to be 1.11–1.30, respectively. The increased value of I_D/I_G for $\text{CoFe}_2\text{O}_4/\text{GO}$ nanocomposites as compared with GO sheets indicates the increase in disorder in GO sheets resulting from the incorporation of CoFe_2O_4 magnetic nanoparticles. The inter-distance (L_D) between Raman active defects is estimated using Tuinstra-Koenig relation [38, 39].

$$\frac{I_D}{I_G} = \frac{C(\lambda)}{L_D}$$

where $C(\lambda) = (2.4 \times 10^{-10} \text{ nm}^{-3}) \lambda^4$ is a constant, and in this case $\lambda = 514 \text{ nm}$, i.e., the excitation wavelength. The inter-defect distance of GO and $\text{CoFe}_2\text{O}_4/\text{GO}$ nanocomposites is calculated to be 15 and 13 nm, respectively. With $L_D > 10 \text{ nm}$, one can expect the variation in I_D/I_G ratio is due to scattered Raman active defects only. The defect density ' n_D ' is calculated using the relation [40].

$$n_D (\text{cm}^{-1}) = 10^{14} / \pi L_D^2$$

and is found to be $1.88 \times 10^{25} / \text{cm}^2$ for nanocomposites, thus indicating a 30% increase in point defects in GO due to nucleation of CoFe_2O_4 nanocrystallites on it.

The observed blue shift in the D and G Raman peaks and increase in FWHM confirm the occurrence of charge transfer between the GO sheets and CoFe_2O_4 NPs. The study of charge transfer interactions of graphene with various electron donors and acceptors is reported in the literature [19, 20]. Charge transfer studies in $\text{CoFe}_2\text{O}_4/\text{GO}$ and particularly its correlation with surface electronic behavior have not been reported till date. In this report, observed blue shift in G peak of GO is attributed to the situation where electron donor nanoparticles get adsorbed. The charge transfer in these nanocomposites also has some effect on Fermi energy level of the material which was quantified from scanning Kelvin probe studies.

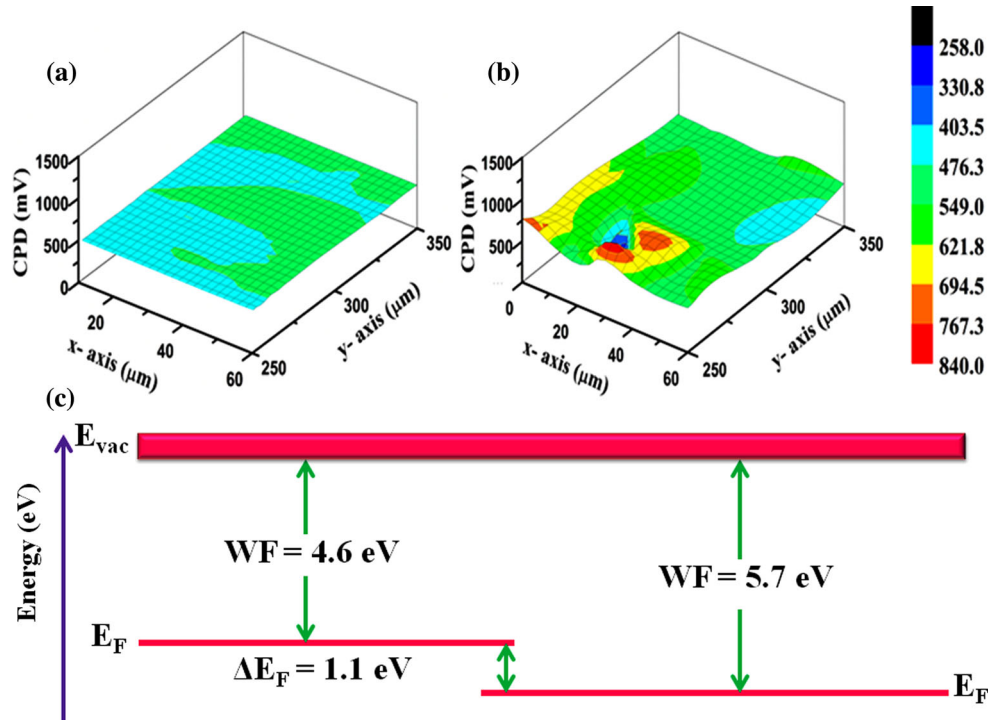
Scanning Kelvin probe studies

The scanning Kelvin probe microscopy was used to study the surface potential and Fermi energy level of GO and $\text{CoFe}_2\text{O}_4/\text{GO}$ nanocomposites. In graphene oxide, Fermi level lies at Dirac point similar to that in graphene. But, in the case of $\text{CoFe}_2\text{O}_4/\text{GO}$ nanocomposites where MNPs are spread over GO sheets, the Fermi level of GO is expected to be changed noticeably by the charge transfer between GO and CoFe_2O_4 NPs. Fermi energy level of any material is related to its work function (WF) by the equation.

$$\Phi_{\text{sample}} = \chi_s + (E_C - E_F) \quad (4)$$

where χ_s is the electron affinity of the sample and E_C and E_F are the conduction band energy and Fermi

Figure 8 CPD mapping of **a** GO and **b** CoFe₂O₄/GO and **c** shifting of Fermi level in nanocomposites.



energy of the material, respectively [41]. Estimation of Fermi level shifting is carried out in terms of work function using scanning Kelvin probe microscopy (SKPM) setup. The WF value of the GO sheets is measured in terms of surface potential or contact potential difference (CPD) between GO and the reference Au tip (WF = 5.1 eV). The CPD mappings of GO and CoFe₂O₄/GO nanocomposites are shown in Fig. 8. Average value of CPD is given by

$$V_{\text{CPD}} = \frac{1}{e} (\Phi_{\text{tip}} - \Phi_{\text{sample}}) \tag{5}$$

where Φ_{tip} and Φ_{sample} are the work functions of tip and sample surface, respectively, and ‘*e*’ is the elementary charge on an electron [42, 43].

The measured average CPD value of GO sheet is found to be 514 mV which corresponds to WF of 4.6 eV. In the case of CoFe₂O₄/GO nanocomposites, obtained average CPD is –610 mV. For simplicity in plotting, the absolute value of CPD has been taken into account as shown in Fig. 8b. The change in contact surface potential must have emancipated from charge transfer between GO and CoFe₂O₄. Using Eq. 5, the average work function of CoFe₂O₄/GO nanocomposites is found to be 5.7 eV. The significant change in the work function value of GO after decoration of CoFe₂O₄ nanoparticles confirms the shifting of Fermi energy level toward valence

band as shown in Fig. 8c. This shifting is due to electron transfer from GO to CoFe₂O₄ which is also envisaged from changes in Raman spectra.

Conclusion

Dispersion of CoFe₂O₄ nanoparticles on GO sheets involves interfacial compressive stress as well as charge transfer between host GO sheets and CoFe₂O₄ magnetic nanoparticles. The superparamagnetic behavior of these nanocomposites is confirmed from its high value of magnetic saturation with *M_s* (75.37 emu/g) and low coercivity value with *H_c* (0.41 kOe), thus indicating soft magnetic nature of CoFe₂O₄/GO nanocomposites. Charge transfer process induces a blue shift in *E_{2g}* phonon as well as an increase in FWHM of Raman spectra of GO sheets. Compressive strain calculated from XRD peak is related to the observed blue shift in Raman peak. Point defects generated in these nanocomposites are of the order of 10²⁵/cm² which play an important role for generation of interfacial compressive stress as well as charge transfer process. The effect of charge transfer is quantified in terms of changes in surface potential of GO, leading to a shift in Fermi surface toward valence band.

Acknowledgements

The authors are thankful to AIRF, JNU, New Delhi, for providing XRD, SEM, TEM characterizations. Authors gratefully acknowledge Dr. R.J. Choudhary of IUC, Indore, for SQUID measurement. Amodini Mishra is thankful to UGC for providing fellowship.

References

- [1] Geim AK, Novoselov KS (2008) The rise of graphene. *Nat Mater* 6:183–191
- [2] Geim AK (2009) Graphene: status and prospects. *Science* 324:1530–1534
- [3] Lv W, Tang Sun F, Fang D-M, Liu H-T, Yang C, Cheng Q-H (2011) A sandwich structure of graphene and nickel oxide with excellent supercapacitive performance. *J Mater Chem* 21:9014–9019
- [4] Dreyer DR, Park S, Bielawski CW, Ruoff RD (2011) The chemistry of graphene oxide. *Chem Soc Rev* 39:228–240
- [5] Zhu BY, Murali S, Cai W, Li X, Suk JW, Potts JR (2010) Graphene and graphene oxide: synthesis, properties, and applications. *Adv Mater* 22:3906–3924
- [6] Rodier BJ, Mosher EP, Burton ST, Matthews R, Pentzer E (2016) Polythioether particles armored with modifiable graphene oxide nanosheets. *Macromol Rapid Commun* 37:894–899
- [7] Cao J, Wang Y, Zhou Y, Ouyang J-H, Guo DJL (2013) High voltage asymmetric supercapacitor based on MnO and graphene electrodes. *J Electroanal Chem* 689:201–206
- [8] Zhou K, Zhu Y, Yang X, Li C (2011) Preparation and application of mediator-free H₂O₂ biosensors of graphene-Fe₃O₄ composites. *Electroanalysis* 23(4):862–869
- [9] Liu BJ, Bai H, Wang Y, Liu Z, Zhang X, Sun DD (2010) Self-assembling TiO₂ nanorods on large graphene oxide sheets at a two-phase interface and their anti-recombination in photocatalytic applications. *Adv Funct Mater* 20:4175–4181
- [10] Chen D, Feng H, Li J (2012) Graphene oxide: preparation, functionalization, and electrochemical applications. *Chem Rev* 112:6027–6053
- [11] Wiedwald U, Ziemann P (2010) Preparation, properties and applications of magnetic nanoparticles. *Beilstein J Nanotechnol* 1:21–23
- [12] Hola K, Markova Z, Zoppellaro G, Tucek J, Zboril R (2015) Tailored functionalization of iron oxide nanoparticles for MRI, drug delivery, magnetic separation and immobilization of biosubstances. *Biotechnol Adv* 33:1162–1176
- [13] Erdem D, Bingham NS, Heiligtag FJ, Pilet N, Warnicke P, Heyderman LJ, Niederberger M (2016) CoFe₂O₄ and CoFe₂O₄-SiO₂ nanoparticle thin films with perpendicular magnetic anisotropy for magnetic and magneto-optical applications. *Adv Funct Mater* 26:1954–1963
- [14] Mansori F, Amiri G, Fatemi M (2016) Synthesis and tissue distribution of CoFe₂O₄ nanoparticles coated with DMSA in rat's liver. *Nanomed J* 3:196–201
- [15] Yuan H, Jiao Q, Zhang Y, Zhang J, Wu Q, Zhao Y, Neerunjun S, Li H (2016) Magnetic CoFe₂O₄ nanoparticles supported basic Poly (Ionic Liquid) catalysts: preparation and catalytic performance comparison in trans esterification and Knoevenagel condensation. *Catal Lett* 146:951–959
- [16] Ma S, Zhan S, Jia Y, Zhou Q (2015) Highly efficient antibacterial and Pb(II) removal effects of AgCoFe₂O₄-GO nanocomposite. *ACS Appl Mater Interfaces* 7:10576–10586
- [17] Fu Y, Chen H, Sun X, Wanga X (2012) Combination of cobalt ferrite and graphene: high performance and recyclable visible-light photocatalysis. *Appl Catal B Environ* 280:111–112
- [18] Li X, Feng J, Du Y, Bai J, Fan H, Zhang H, Peng Y, Li F (2015) One-pot synthesis of CoFe₂O₄/graphene oxide hybrids and their conversion into FeCo/graphene hybrids for lightweight and highly microwave absorber. *J Mater Chem A* 3:5535–5546
- [19] Kumar PR, Kollu P, Santosh C, Rao KEV, Kim DK, Grace AN (2014) Enhanced properties of porous CoFe₂O₄-reduced graphene oxide composites with alginate binders for Li-ion battery applications. *N J Chem* 38:3654–3666
- [20] Ramachandran R, Mani V, Chen S-M, Saraswathi R, Lou B-S (2013) Recent trends in graphene based electrode materials for energy storage devices and sensors applications. *Int J Electrochem Sci* 8:11680–11694
- [21] Morones JR, Elechiguerra JL, Camacho A, Holt K, Kouri JB, Ramirez JT, Yacaman MJ (2005) The bactericidal effect of silver nanoparticles. *Nanotechnology* 16:2346–2353
- [22] Wang G, Ma Y, Wei Z, Qi M (2016) Development of multifunctional cobalt ferrite/graphene oxide nanocomposites for magnetic resonance imaging and controlled drug delivery. *Chem Eng J* 289:150–160
- [23] Mishra A, Mohanty T (2016) Structural and morphological study of magnetic Fe₃O₄/reduced graphene oxide. *Mater Today Proc* 3:1576–1581
- [24] Lee SC, Some S, Kim SW, Kim SJ, Seo J, Lee J, Lee T, Ahn JH, Choi HJ, Jun SC (2015) Efficient direct reduction of graphene oxide by silicon substrate. *Sci Rep* 5:12306–12315
- [25] Turtelli RS, DuongG V, Nunes W, GrossingerR Knobel M (2008) Magnetic properties of nanocrystalline CoFe₂O₄ synthesized by modified citrate-gel method. *J Magn Magn Mater* 320:e339–e342
- [26] Wang G, Ma Y, Dong X, TongY Zhang L, Mu J, Bai Y, Hou JY, Che H, Zhang X (2015) monodisperse

- Polyvinylpyrrolidone-coated CoFe_2O_4 nanoparticles: synthesis, characterization and cytotoxicity study. *Appl Surf Sci* 357:2131–2135
- [27] Dutta P, Seehra M, Thota S, Kumar J (2007) A comparative study of the magnetic properties of bulk and nanocrystalline Co_3O_4 . *J Phys Condens Matter* 20:015218–015228
- [28] Ragasudha M, Ravinder D, Veerasomaiah P (2016) Investigation of superparamagnetism in pure and chromium substituted cobalt nanoferrite. *J Magn Magn Matter* 420:45–50
- [29] Williamson GK, Hall WH (1953) X-ray line broadening from field aluminum and wolfram. *Acta Metall* 1:22–31
- [30] Mishra A, Choudhary SN, Choudhary RNP, Murthy VRK, Prasad K (2012) Dielectric relaxation in complex perovskite $\text{Ba}(\text{Bi}_{1/2}\text{Ta}_{1/2})\text{O}_3$. *J Mater Sci Mater Electron* 23:185–192
- [31] Ferrari AC, Meyer JC, Scardai V, Casiraghi C, Lazzeri M, Mauri F, Piscanes S, Jiang D, Novoselov KS, Roth S, Geim AK (2006) Raman spectrum of graphene and graphene layers. *Phys Rev Lett* 97:187401–187404
- [32] Ferrari AC, Robertson J (2000) Interpretation of Raman spectra of disordered and amorphous carbon. *Phys Rev B* 61:14095–14107
- [33] Li Z, Young RJ, Kinloch IA (2013) Interfacial stress transfer in graphene oxide nanocomposites. *ACS Appl Mater Interfaces* 5:456–463
- [34] Zheng X, Chen W, Wang G, Yu Y, Qin S, Fang J, Wang F, Zhang X-A (2015) The Raman red shift of graphene impacted by gold nanoparticles. *AIP Adv* 5:057133–057136
- [35] Parlevliet PP, Bersee ENH, Beukers A (2007) Residual stresses in thermoplastic composites—a study of the literature, part III: effects of thermal residual stresses. *Compos A* 38:1581
- [36] Mishra A, Mohanty T (2016) Analysis of surface potential and magnetic properties of Fe_3O_4 /graphene oxide nanocomposites. *AIP Conf Proc* 050010:1731
- [37] Ni ZH, Wang HM, Ma Y, Kasim J, Wu YH, Shen ZX (2008) Tunable stress and controlled thickness modification in graphene by annealing. *ACS Nano* 5:1033–1039
- [38] Tuinstra F, Koenig JL (1970) Raman spectrum of graphite. *J Chem Phys* 53:1126–1130
- [39] Mishra M, Meinerzhagen F, Schleberger M, Kanjilal D, Mohanty T (2015) Swift heavy ion induced optical and electronic modifications of graphene– TiO_2 nanocomposites. *J Phys Chem C* 119:21270–21277
- [40] Cancado LG, Jorio A, Ferreira EHM, Stavale F, Achete CA, Capaz RB, Moutinho MVO, Lombardo A, Kulmala TS, Ferrari AC (2011) Quantifying defects in graphene via Raman spectroscopy at different excitation energies. *Nano Lett* 11:3190–3196
- [41] Kumar A, Mohanty T (2014) Electro-optic modulation induced enhancement in photocatalytic activity of N-doped TiO_2 thin films. *J Phys Chem C* 118:7130–7138
- [42] Sadewasser S, Leendertz C, Streicher F, Lux-Steiner MC (2009) The influence of surface topography on Kelvin probe force microscopy. *Nanotechnology* 20:505503–505513
- [43] Cheran L-E, Thompson M, Liess H-D (1999) Scanning Kelvin microprobe in the tandem analysis of surface topography and chemistry. *Analyst* 124:961–970